Comput Mech (2007) 40:651–666
DOI 10.1007/s00466-006-0131-0

ORIGINAL PAPER

Mechanics of extended continua: modeling and simulation of elastic microstretch materials

N. Kirchner · P. Steinmann

Received: 26 April 2006 / Accepted: 25 September 2006 / Published online: 10 November 2006

Abstract The investigation of microstretch and micromorphic continua (which are prominent examples of so-called extended continua) dates back to Eringens pioneering works in the mid 1960, cf. (Eringen in Mechanics of micromorphic materials. Springer, Berlin Heidelberg New York, pp 131–138, 1966; Eringen in Int J Eng Sci 8:819–828; Eringen in Microcontinuum field theories. Springer, Berlin Heidelberg New York, 1999). Here, we re-derive the governing equations of microstretch continua in a variational setting, providing a natural framework within which numerical implementations of the model equations by means of the finite element method can be obtained straightforwardly. In the application of Dirichlets principle, the postulation of an appropriate form of the Helmholtz free energy turns out to be crucial to the derivation of the balance laws and constitutive relations for microstretch continua. At present, the material parameters involved in the free energy have been assigned fixed values throughout all numerical simulations—this simplification is addressed in detail as the influence of those parameters must not be underestimated. Since only few numerical results demonstrating elastic microstretch material behavior in engineering applications are available, the focus is here on the presentation of numerical results for simple twodimensional test specimens subjected to a plane strain condition and uniaxial tension. Confidence in the simulations for microstretch materials is gained by showing that they exhibit a "downward-compatibility" to Cosserat continuum formulation: by switching off all stretch-related effects, the governing set of equations reduces to the one used for polar materials. Further, certain material parameters can be chosen to act as penalty parameters, forcing stretch-related contributions to an almost negligible range in a full microstretch model so that numerical results obtained for a polar model can be obtained as a limiting case from the full microstretch model.

Keywords Microstretch continua · Variational approach · Finite element method · Elasticity

N. Kirchner (✉)
Department of MDF, Fraunhofer-Platz 1, Fraunhofer ITWM, 67663 Kaiserslautern, Germany
e-mail: nina.kirchner@itwm.fraunhofer.de

P. Steinmann
Chair of Applied Mechanics, University of Kaiserslautern, 67653 Kaiserslautern, Germany
e-mail: ps@rhrk.uni-kl.de

1 Introduction and outline

Microstretch continua belong to the class of micromorphic continua introduced by Eringen (in e.g. [12,14, 15,17] and cumulatively summarized and extended by Eringen in [18]) and by Mindlin (in [34], where in the latter, the terminology "micromorphic" is, however, not used).

In order to set the stage for the subsequent investigations, and, also, to determine the "location" of microstretch theory relative to other continuum field theories, let us recall that in the standard Boltzmann continuum, each material point is solely characterized by its mass and has three translational degrees of freedom. Typically, macroscopic descriptions of e.g. engineering materials (steels, concrete, ceramics, fluids etc.), geomaterials (such as soils, rocks, ice), or biomaterials (bones, tissues, blood) are based on a Boltzmann continuum. However, it is well known that complex materials

such as e.g. monodisperse media can not adequately be described using Boltzmann continuum theories, since the rotational motion of individual grains gives rise to an additional dynamic field called intrinsic spin.

Thus, a general continuum theory accounting for the intrinsic rotational motion has been proposed in [6] and re-discovered e.g. in [13,19,21,22,47,48]—it is today known as Cosserat theory, or, polar theory. In this theory, a material point is characterized by its mass and by microstructural properties described by a *rigid* triad of vectors (the so-called directors) attached to each point so that consequently, each material point has three translational and three rotational degrees of freedom. Today, polar theory is commonly used in macroscopic descriptions of materials with rigid microstructure[1] including liquid crystals, polymer suspensions, granular media, and porous materials, see for instance [7,10,32]. Moreover, micropolar continuum formulations have in the last decades been intensively studied within the context of localization computations. It has been discovered that in the numerical modeling of the behavior of e.g. strain softening materials, the independent rotational degree of freedom introduced as an amendment to the standard Boltzmann continuum has a regularizing effect in the sense that the pathological mesh dependence of the post–peak response (which is observed for implementations based on the standard continuum formulation) is overcome, see e.g. [8,11,35,36]. While the independent rotational degree of freedom is obviously activated under shearing loads, it is certainly inactive when tensile loads are applied. Consequently, one can in general not expect to benefit from the regularizing effect of the independent rotational degree of freedom if numerical schemes based on polar theory are used to solve problems dominated by the application of tensile loads. Besides capturing size effects, it is well-known that the inclusion of higher gradients in the constitutive modeling is a physically motivated option to regularize the pathological mesh dependence in inelastic softening computations, cf. e.g. [1,8,10,11,35,36,45]. In many of these cases a micropolar description based on the Cosserat-approach ([6]) is applied for the regularization of shear-localization, in particular for granular materials. Nevertheless it turns out that the inclusion of the curvature does not provide for a regularization of tensile-localization, cf. [11]. This in turn can be achieved e.g. in 1d by the inclusion of the gradient of the normal strain, which is demonstrated repeatedly in the localization community for the examples of brittle and ductile materials. For isotropic gradient damage the regularizing effect is demonstrated e.g. in [46]. The microstretch approach thus clearly promises to combine the benefits of the two above approaches when it comes to the regularization of localization both in shear and tension.

If the deformation of the microstructure is no longer regarded as rigid—as is the case for polar media—but restricted to an inflation (expansion) or contraction (compression), that is, if we consider continuous materials with isotropically deforming microstructure such as e.g. bubbly liquids and porous foams (where bubbles/voids inflate and collapse), the so-called microstretch continuum theory provides the proper framework for a theoretical description and analysis of those media. In microstretch materials, each material point is thus characterized by its mass and by microstructural properties described by an *isotropically deformable* triad of vectors attached to each point—consequently, a material point has three translational, three rotational and one stretching degree of freedom. After Eringens pioneering work [12] in the 1960s, recent interest in the theory of elastic microstretch materials arouse from the 1990s on when issues related to the problem of stress concentrations (around a circular hole and around a rigid inclusion, see e.g. [9,27]), the propagation of waves (see e.g. [29,43]), the thermomechanical coupling (see e.g. [16]), the existence and uniqueness of solutions to the static (linear) boundary value problem as well as to the bending problem of homogeneous, isotropic plates (see e.g. [5,24,26]) and to deformations of anisotropic microstretch materials (see [40]) have been investigated. All those cited works have in common that they take the balance equations for microstretch materials as derived by Eringen as a starting point; moreover, they are written in a primarily mathematically spirit,[2] so that we here take the opportunity to re-derive the balance equations using an alternative approach which is simultaneously particularly suited to be used for numerical investigations.

In the long run, we are interested in the question of whether numerical computations for e.g. elastoplastic strain softening microstretch materials turn out to be mesh independent irrespective of whether shear loads (which obviously activate the independent rotational degree of freedom) or tensile loads (which activate the independent stretching degree of freedom) are applied. However, in order to do one step at a time, we shall in the present article only be concerned with elastic microstretch material behavior as this already provides ample

[1] Obviously, the description of continua which are characterized by a *deformable* microstructure such as e.g. materials with changing porosity is beyond the scope of a polar theory.

[2] The mathematical analysis of microstretch solids is at present restricted to the static case and linear elastic bodies in an infinitesimal theory.

opportunity to get acquainted with phenomena related to the additional microstretch degree of freedom. The theoretical and numerical analysis as well as the algorithmic treatment of inelastic microstretch material behavior (e.g. in the framework of an associative deviatoric elastoplasticity) including strain softening phenomena is the subject of a subsequent article.

The structure of the present article is organized as follows: after introducing notation in Sect. 2, the balance equations governing an elastic microstretch continua are derived in the framework of a variational principle. Further, constitutive relations describing hyperelastic material behavior are addressed. The discretization of the resulting system of differential equations is described in Sect. 3, so that we can turn to the presentation of numerical examples for elastic microstretch materials in Sect. 4. Finally, Sect. 5 contains conclusions and an outlook.

Remark 1 Unfortunately, materials with unconstrainedly deforming microstructure such as metallic foams (where general changes in porosity are due to e.g. the opening of new channels which may stretch, wring, inflate and be distorted) or suspensions of deformable long chain polymers can still not be described by microstretch theory. So, finally, the so-called micromorphic theory has been designed (see again e.g. [14,15,17,18,34]) to account for all possible deformations of a microstructure, not just isotropic ones. In a micromorphic theory, each material point possesses (in addition to its three translational degrees of freedom) nine additional degrees of freedom. While most investigations of micromorphic continua are limited to elastic material behavior under static conditions and at infinitesimal strains, recent progress in the realm of constitutive modeling has been achieved by Forest and Sievert in [20], dealing with viscoplastic micromorphic material behavior. A constitutive theory for micromorphic thermoplasticity has been suggested by Lee and Chen [31], but still awaits its numerical implementation. On the mathematical side, Neff [38] has recently presented general existence theorems for elastic, micromorphic continua subject to finite strain conditions. For the case of linear, dynamic micromorphic elasticity, Iesan and Nappa [25] have established existence and uniqueness theorems, while Nappa [37] establishes variational principles which fully characterize the solution of initial boundary value problems of linear, dynamic micromorphic thermoelasticity. In order to pave the way for the development of efficient algorithms to be used for forthcoming comprehensive numerical investigations of micromorphic continua, a unifying discussion of variational principles for gradient and micromorphic continua has recently been presented in [28], focusing in particular on the considerable influence of the theoretical results derived on forthcoming numerical implementations.

2 Variational principle

2.1 Notation

To set the stage, let us introduce some notation. Unless otherwise stated, vectors and tensors of rank 2 will throughout this article be denoted by small, bold letters. A dot $(\cdot)$ is used to indicate the contraction over one index, so that we have $\boldsymbol{a}\cdot\boldsymbol{b}=a_ib_i$ $(\forall\, i,j=1,2,3,\ \boldsymbol{a},\boldsymbol{b}\in\mathbb{R}^3)$, $(\boldsymbol{a}\cdot\boldsymbol{b})_i=a_{ij}b_j$ $(\forall\, i,j=1,2,3,\ \boldsymbol{a}\in\mathbb{R}^3\times\mathbb{R}^3,\boldsymbol{b}\in\mathbb{R}^3)$ and $(\boldsymbol{a}\cdot\boldsymbol{b})_{ik}=a_{ij}b_{jk}$ $(\forall i,j,k=1,2,3$ and $\boldsymbol{a},\boldsymbol{b}\in\mathbb{R}^3\times\mathbb{R}^3)$. Moreover, the contraction of a tensor of rank 3 and a vector is given by e.g. $(\boldsymbol{\epsilon}\cdot\boldsymbol{a})_{ij}=\epsilon_{ijk}a_k$. In these relations, Einsteins summation convention is used throughout. The complete contraction of two tensors of rank 2 is denoted by a double dot, (:), i.e. $\boldsymbol{a}:\boldsymbol{b}=a_{ij}b_{ij}\ \forall i,j=1,2,3$ and $\boldsymbol{a},\boldsymbol{b}\in\mathbb{R}^3\times\mathbb{R}^3$. The twofold contraction of a tensor of rank 4, say $\mathcal{J}$, and a tensor of rank 2 is given by $(\mathcal{J}:\boldsymbol{a})_{ij}=\mathcal{J}_{ijkl}a_{kl}$. The dyadic product of two tensorial quantities is represented by the symbol $\otimes$.

Special quantities encountered throughout the article are $\boldsymbol{I},\mathbb{J},\mathbb{J}^{\mathsf{sym}}$ and $\mathbb{J}^{\mathsf{skw}}$ denoting the second-order, the fourth-order, the symmetric fourth-order and the skew-symmetric fourth order identity tensors with components δ_{ij}, $\delta_{ik}\delta_{jl}$, $(\delta_{ik}\delta_{jl}+\delta_{il}\delta_{jk})/2$, $(\delta_{ik}\delta_{jl}-\delta_{il}\delta_{jk})/2$, respectively. Moreover, we define the symmetric fourth-order deviatoric and volumetric operators as follows: $\mathbb{J}^{\mathsf{dev}}=\mathbb{J}^{\mathsf{sym}}-\mathbb{J}^{\mathsf{vol}}$ where $\mathbb{J}^{\mathsf{vol}}=(\boldsymbol{I}\otimes\boldsymbol{I})/3$. With the help of these definitions, we observe that any 2-tensor $\boldsymbol{a}$ can be decomposed additively into its volumetric, symmetric deviatoric and skew-symmetric part, viz. $\boldsymbol{a}=\mathbb{J}^{\mathsf{vol}}:\boldsymbol{a}+\mathbb{J}^{\mathsf{dev}}:\boldsymbol{a}+\mathbb{J}^{\mathsf{skw}}:\boldsymbol{a}$. Furthermore, $\boldsymbol{\epsilon}$ is the third-order Ricci tensor (permutation tensor), while spn denotes the spin-operator. Applied to a vector $\boldsymbol{a}$, it yields $\operatorname{spn}\boldsymbol{a}=-\boldsymbol{\epsilon}\cdot\boldsymbol{a}$, or, in index-notation, $(\operatorname{spn}\boldsymbol{a})_{ij}=-\epsilon_{ijk}a_k$.

As usual, the material body under consideration is viewed as a subset of the Euclidean space $\mathbb{R}^3$, is denoted by $\mathcal{V}$ and has boundary $\partial\mathcal{V}$ with outward unit normal vector $\boldsymbol{n}$. The particles (or, material points) contained within $\mathcal{V}$ are labeled by $\boldsymbol{x}$, and all further quantities introduced will also be referred to the configuration $\mathcal{V}$. Since we work here for simplicity in a geometrically linear setting, the displacement field

$$\boldsymbol{u}=\boldsymbol{u}(\boldsymbol{x}):\mathcal{V}\to\mathbb{R}^3 \tag{1}$$

is one of the primary independent variables which will later have to be determined by solving (numerically) the governing equations of microstretch continua.

Moreover, we introduce the independent vector-valued field of rotation and the independent scalar-valued field of microstretch,

$$\boldsymbol{\omega} = \boldsymbol{\omega}(\boldsymbol{x}) : \mathcal{V} \to \mathbb{R}^3, \quad \xi = \xi(\boldsymbol{x}) : \mathcal{V} \to \mathbb{R}. \tag{2}$$

To be able to account for short-range non-local effects in the material behavior, we further introduce

$$\boldsymbol{\kappa} := \nabla_{\boldsymbol{x}} \boldsymbol{\omega}\,, \quad (\kappa_{ij} = \omega_{i,j}) \qquad \boldsymbol{\tau} := \nabla_{\boldsymbol{x}} \xi \quad (\tau_i = \xi_{,i}) \tag{3}$$

and refer to $\boldsymbol{\kappa}$ and $\boldsymbol{\tau}$ as the curvature tensor and the stretch gradient, respectively.

2.2 General remarks

A variational approach to describe micromorphic continua has been presented by Mindlin more then 40 years ago, see [34]. There, rather then restricting attention to stationary conditions and applying Dirichlet's principle, the stress equations of motion have been deduced in a geometrically linear setting by defining a Lagrangian and adopting Hamilton's principle. A closer re-investigation of variational principles applied in the 1960s to micromorphic and so-called "second-gradient-of strain models" is given in [28], where apart from the standard Dirichlet principle and the restriction to the geometrically linear setting also mixed (regularized) variational formulations and a geometrically non-linear setting are considered. The emphasis in [28] is on an identification of the inherent properties of the deduced balance equations for higher gradient and micromorphic continua with regard to subsequent implementations into e.g. FEM codes.

Specializing and continuing the analysis presented in [28], we will here again apply Dirichlet's principle and modify the so-called micropolar Dirichlet principle proposed in [45] in a suitable manner to derive the balance equations for microstretch materials. As expected, the microstretch Dirichlet principle proposed here turns out to be a specialization of the micromorphic Dirichlet principle investigated in [28]. Eringen, in contrast, deduces in his works [16–18] the corresponding equations by considering invariance properties of (a modified) energy balance. It will be seen that upon postulating an appropriate form of the (Helmholtz) free energy, we get exactly the same balance equations as e.g. in [18].

Remark 2 In mechanics as well as in mathematics, variational principles have been used for more than two centuries. Historical comments on the role of variational principles in mechanics can e.g. be found in [39] where also more detailed bibliographical information is gathered. The Dirichlet Principle, which is here in the focus of our attention, states that any field $\boldsymbol{u}$ minimizing the potential energy of a system under consideration is also a solution of the corresponding Euler–Lagrange equations (also known as the balance equations) associated to this system. Moreover, the converse is true so that fields which are solutions of the balance equations minimize the potential energy Π. In mechanics, the Dirichlet Principle is hence also referred to as the principle of minimum potential energy, yielding the equilibrium conditions for static, elastic bodies, see [39]. Mathematically, the equivalence of the two statements "$\Pi(\boldsymbol{u})$ is minimal" and "$\boldsymbol{u}$ satisfies the Euler–Lagrange equations" is established under quite general conditions in a functional analytic framework in the theorem of Lax and Milgram, see [30].

The application of variational principles in mechanics has two outstanding features that make this approach favorable against other ones:[3] as mentioned above, balance equations are derived, and, in addition, constitutive relations describing elastic material behavior are obtained as a by-product of the variational analysis. Should we wish to model e.g. elastoplastic material behavior, the elastic constitutive relations deduced from the variational approach have to be complemented by evolution equations for e.g. the plastic strain which, usually, are obtained by invoking the principle of maximum plastic dissipation, see e.g. [23]. Moreover, the variational formulation provides a natural framework within which a numerical implementation of the model equations by means of the finite element method is conceptually relatively easy obtained.

2.3 Balance laws and constitutive relations describing elastic microstretch continua

For simplicity, we restrict attention to hyperelastic material behavior in conservative systems and assume the existence of a total potential energy Π under (quasi)static conditions, which is consisting of two contributions, viz.

$$\Pi := \hat{\Pi}(\boldsymbol{u}, \boldsymbol{\omega}, \xi) = \Pi^{\text{int}}(\boldsymbol{u}, \boldsymbol{\omega}, \xi) + \Pi^{\text{ext}}(\boldsymbol{u}, \boldsymbol{\omega}, \xi)\,. \tag{4}$$

Extending the micropolar Dirichlet Principle investigated in [45], we specify Π^{int} with the help of the free

[3] An alternative approach is to deduce the balance equations from first principles and to establish constitutive relations by exploiting entropy principles—this is known as the rational mechanics approach and which has been established by Truesdell and Noll in [49].

(Helmholtz) energy ψ as (ρ is the mass density)

$$\Pi^{\text{int}} := \int_{\mathcal{V}} \rho\psi\Big(\mathbb{J}^{\text{sym}} : \nabla_{\boldsymbol{x}}\boldsymbol{u}, \mathbb{J}^{\text{skw}} : \nabla_{\boldsymbol{x}}\boldsymbol{u} + \boldsymbol{\epsilon}\cdot\boldsymbol{\omega}, \nabla_{\boldsymbol{x}}\boldsymbol{u} : \boldsymbol{I} - \xi, \boldsymbol{\kappa}, \boldsymbol{\tau}\Big)\,\mathrm{d}v\,, \tag{5}$$

while we let

$$\Pi^{\text{ext}} := -\int_{\mathcal{V}} \rho[\boldsymbol{f}_u\cdot\boldsymbol{u} + \boldsymbol{f}_{\boldsymbol{\omega}}\cdot\boldsymbol{\omega} + f_\xi\xi]\,\mathrm{d}v - \int_{\partial\mathcal{V}} [\boldsymbol{t}_{\boldsymbol{u}}\cdot\boldsymbol{u} + \boldsymbol{t}_{\boldsymbol{\omega}}\cdot\boldsymbol{\omega} + t_\xi\xi]\,\mathrm{d}a\,. \tag{6}$$

Above, $\boldsymbol{f}_{\boldsymbol{u}}$ and $\boldsymbol{t}_{\boldsymbol{u}}$ are the usual (volume distributed) body force vector (such as e.g. gravitation) and the (surface distributed) traction vector. Moreover, we have postulated volume- and surface-distributed forces associated with the rotation and the stretch, respectively, which are of the form $\boldsymbol{f}_{\boldsymbol{\omega}}$, $\boldsymbol{t}_{\boldsymbol{\omega}}$ and f_ξ, t_ξ.

Remark 3 The introduction of additional body tractions and forces related to the microstructure is carried out in formal analogy to e.g. [2].

In the following, attention is restricted to the consideration of small strains, and the underlying strain measures are chosen as

$$\boldsymbol{\varepsilon} := \nabla_{\boldsymbol{x}}\boldsymbol{u} + \boldsymbol{\epsilon}\cdot\boldsymbol{\omega}, \quad e := \nabla_{\boldsymbol{x}}\boldsymbol{u} : \boldsymbol{I} - \xi. \tag{7}$$

Here, $\boldsymbol{\varepsilon}$ is a Cosserat-type-strain and e is a volumetric strain referred to as the effective dilatation, cf. also [44]. Note that e combines micro- and macroscale effects and can hence (namely by a simple change of sign) provide information about whether macroscopic effects dominate microscale influences rooting in the stretching degree of freedom ($e > 0$) or vice versa. Since the arguments of free energy ψ are given by the symmetric gradient of the displacement ($\mathbb{J}^{\text{sym}} : \nabla_{\boldsymbol{x}}\boldsymbol{u}$), the relative strain e and a gradient of the microstructural field quantity ($\boldsymbol{\tau} = \nabla_{\boldsymbol{x}}\xi$), the representation (5) is in fact a specification of its general form used to model micromorphic continua, see [28]. What is however additionally accounted for in (5) are the arguments stemming from considering independent rotations, i.e. $\mathbb{J}^{\text{skw}} : \nabla_{\boldsymbol{x}}\boldsymbol{u} + \boldsymbol{\epsilon}\cdot\boldsymbol{\omega}$ and $\boldsymbol{\kappa} = \nabla_{\boldsymbol{x}}\boldsymbol{\omega}$. Although accounting for those rotation related fields requires a more complicated analysis than e.g. carried out for microstretch materials without independent rotations (in which case (5) could be viewed as a direct specialization of its counterpart given in [28]), it has the advantage that the results to be derived can easily be compared to existing results deduced e.g. for micropolar materials in [45] (namely by switching off all stretch related effects).

Expressing the principle of minimal potential energy as

$$\delta\Pi(\bullet) = \frac{\mathrm{d}}{\mathrm{d}\alpha}\Big(\Pi\big((\bullet) + \alpha\delta(\bullet)\big)\Big)\Big|_{\alpha=0} \stackrel{!}{=} 0\,, \tag{8}$$

where δ denotes the variation and $\alpha \in \mathbb{R}$ is a small parameter, an exploitation of (8) yields – since the variations $\delta_{\boldsymbol{u}}$, $\delta_{\boldsymbol{\omega}}$ and δ_ξ are arbitrary and independent of each other and we tacitly assume sufficient smoothness of the fields involved—the following balance equations:

$$\mathsf{div}\,(\boldsymbol{\sigma}^{\mathsf{t}} + s\boldsymbol{I}) + \rho\boldsymbol{f}_{\boldsymbol{u}} = \boldsymbol{0} \quad \text{in } \mathcal{V}, \tag{9}$$

$$\boldsymbol{\epsilon} : \boldsymbol{\sigma} + \mathsf{div}\,\boldsymbol{m}^{\mathsf{t}} + \rho\boldsymbol{f}_{\boldsymbol{\omega}} = \boldsymbol{0} \quad \text{in } \mathcal{V}, \tag{10}$$

$$s + \mathsf{div}\,\boldsymbol{\lambda} + \rho f_\xi = 0 \quad \text{in } \mathcal{V}. \tag{11}$$

Here, the superscript t denotes the transpose of a 2-tensor, while the symbol div is the divergence-operator acting on the last index of a 2-tensor. Note that the total stress $\boldsymbol{\sigma}^{\text{total}}$ entering the balance of linear momentum is given by $\boldsymbol{\sigma}^{\text{total}} = \boldsymbol{\sigma} + s\boldsymbol{I}$, that is, it is additively composed of the bulk (Cauchy) stress $\boldsymbol{\sigma}$ and the microscopic stress $s\boldsymbol{I}$ as arising in the description of compressibility effects of interstitial pore gas in closed cell foams, see e.g. [44].

Provided that we deal with static conditions only, relations (9)–(11) constitute the balances of linear momentum, intrinsic spin and microstretch of an elastic generalized continuum. Equations (9)–(11) are complemented by the boundary conditions

$$[\boldsymbol{\sigma} + s\boldsymbol{I}]^{\mathsf{t}}\cdot\boldsymbol{n} = \boldsymbol{t}_{\boldsymbol{u}}, \quad \boldsymbol{m}^{\mathsf{t}}\cdot\boldsymbol{n} = \boldsymbol{t}_{\boldsymbol{\omega}}, \quad \boldsymbol{\lambda}\cdot\boldsymbol{n} = t_\xi \quad \text{on } \partial\mathcal{V}, \tag{12}$$

derived also from (8) and in which $\boldsymbol{t}_{\boldsymbol{u}}$, $\boldsymbol{t}_{\boldsymbol{\omega}}$ and t_ξ are (generalized) surface tractions associated with the displacement, the rotations and the stretch, respectively. In (9)–(12), $\boldsymbol{\sigma}$ and $\boldsymbol{m}$ are the Cauchy stress and couple stress tensor, respectively, while s and $\boldsymbol{\lambda}$ are referred to as the microstretch pressure and the microstress vector. With the help of the free energy, ψ, these constitutive quantities are defined as

$$\boldsymbol{\sigma}^{\mathsf{t}} := (\mathbb{J}^{\text{vol}} + \mathbb{J}^{\text{dev}} + \mathbb{J}^{\text{skw}}) : \boldsymbol{\sigma}^{\mathsf{t}} := \rho\frac{\partial\psi}{\partial\mathbb{J}^{\text{vol}} : \boldsymbol{\varepsilon}} + \rho\frac{\partial\psi}{\partial\mathbb{J}^{\text{dev}} : \boldsymbol{\varepsilon}} + \rho\frac{\partial\psi}{\partial\mathbb{J}^{\text{skw}} : \boldsymbol{\varepsilon}}\,, \tag{13}$$

$$s := \rho\frac{\partial\psi}{\partial e}\,, \quad \boldsymbol{m}^{\mathsf{t}} := \rho\frac{\partial\psi}{\partial\boldsymbol{\kappa}}\,, \quad \boldsymbol{\lambda} := \rho\frac{\partial\psi}{\partial\boldsymbol{\tau}}\,, \tag{14}$$

and have in fact been obtained as a "by-product" in the course of deducing the Euler–Lagrange Equations (9)–(11).

Remark 4 It is emphasized that the balances of linear momentum and stretch, (9) and (11), are coupled: the total stress in (9) consists of the "usual" Cauchy stress $\boldsymbol{\sigma}$ and the microstretch pressure tensor, $s\boldsymbol{I}$. If the microstretch vanishes identically, $\xi = 0$, we recover the

linear momentum balance in its standard from, while the stretch balance also vanishes. Since the balance of spin remains unaffected, the system (9)–(11) reduces thus for $\xi = 0$ to the standard balance equations for polar materials.

To model linearly elastic microstretch continua, we let the free energy be given by a quadratic function of its arguments listed in (5), viz.

$$\begin{aligned}\rho\psi &= \rho\hat{\psi}(\mathbb{J}^{\mathsf{vol}}:\boldsymbol{\varepsilon},\mathbb{J}^{\mathsf{dev}}:\boldsymbol{\varepsilon},\mathbb{J}^{\mathsf{skw}}:\boldsymbol{\varepsilon},e,\boldsymbol{\kappa},\boldsymbol{\tau})\\ &:= \frac{1}{2}K\big[[\mathbb{J}^{\mathsf{vol}}:\boldsymbol{\varepsilon}]:\boldsymbol{I}\big]^2+\frac{1}{2}K_\xi e^2+\mu\big[[\mathbb{J}^{\mathsf{dev}}:\boldsymbol{\varepsilon}]^2+l^2\boldsymbol{\kappa}^2\big]\\ &\quad+\mu_c[\mathbb{J}^{\mathsf{skw}}:\boldsymbol{\varepsilon}]^2+\frac{1}{2}\pi_\xi\boldsymbol{\tau}^2\,. \end{aligned}\tag{15}$$

where we have used

$$\mathbb{J}^{\mathsf{sym}}:\nabla_{\boldsymbol{x}}\boldsymbol{u}=\mathbb{J}^{\mathsf{vol}}:\nabla_{\boldsymbol{x}}\boldsymbol{u}+\mathbb{J}^{\mathsf{dev}}:\nabla_{\boldsymbol{x}}\boldsymbol{u}=\mathbb{J}^{\mathsf{vol}}:\boldsymbol{\varepsilon}+\mathbb{J}^{\mathsf{dev}}:\boldsymbol{\varepsilon}\tag{16}$$

and

$$(\mathbb{J}^{\mathsf{skw}}:\nabla_{\boldsymbol{x}}\boldsymbol{u})+\boldsymbol{\epsilon}\cdot\boldsymbol{\omega}=\mathbb{J}^{\mathsf{skw}}:(\nabla_{\boldsymbol{x}}\boldsymbol{u}+\boldsymbol{\epsilon}\cdot\boldsymbol{\omega})=\mathbb{J}^{\mathsf{skw}}:\boldsymbol{\varepsilon}\,.\tag{17}$$

In (15), K and K_ξ are the "usual" and the microstretch bulk modulus, respectively, and μ and μ_c denote the shear moduli. Further, l is a characteristic length, while π_ξ is a parameter related to the microstretch. Combining (13) and (14) with (15), we derive explicit constitutive relations of the form

$$\begin{aligned}&\mathbb{J}^{\mathsf{vol}}:\boldsymbol{\sigma}=K\big[[\mathbb{J}^{\mathsf{vol}}:\boldsymbol{\varepsilon}]:\boldsymbol{I}\big]\boldsymbol{I},\quad \mathbb{J}^{\mathsf{dev}}:\boldsymbol{\sigma}=2\mu\mathbb{J}^{\mathsf{dev}}:\boldsymbol{\varepsilon}\,,\\ &\mathbb{J}^{\mathsf{skw}}:\boldsymbol{\sigma}=-2\mu_c\mathbb{J}^{\mathsf{skw}}:\boldsymbol{\varepsilon},\quad s=K_\xi e\,,\\ &\boldsymbol{m}^{\mathsf{t}}=2\mu l^2\boldsymbol{\kappa},\quad \boldsymbol{\lambda}=\pi_\xi\boldsymbol{\tau}.\end{aligned}\tag{18}$$

Therefore, strain $\boldsymbol{\varepsilon}$, effective dilatation e, curvature $\boldsymbol{\kappa}$ and microstretch gradient $\boldsymbol{\tau}$ are connected to the Cauchy stress $\boldsymbol{\sigma}$, the microstretch pressure s, the couple stress $\boldsymbol{m}$ and the microstress $\boldsymbol{\lambda}$ by the continuum elastic tangent operator $\mathbb{T}_{\mathrm{e}}$ as follows:

$$\begin{bmatrix}\boldsymbol{\sigma}\\ \boldsymbol{m}\\ \boldsymbol{\lambda}\\ s\end{bmatrix}^{\mathsf{t}}=\underbrace{\begin{bmatrix}K\boldsymbol{I}\otimes\boldsymbol{I}+2\mu\mathbb{J}^{\mathsf{dev}}+2\mu_c\mathbb{J}^{\mathsf{skw}} & 0 & 0 & 0\\ 0 & 2\mu l^2\boldsymbol{I} & 0 & 0\\ 0 & 0 & \pi_\xi\boldsymbol{I} & 0\\ 0 & 0 & 0 & K_\xi\end{bmatrix}}_{=:\mathbb{T}_{\mathrm{e}}}\begin{bmatrix}\boldsymbol{\varepsilon}\\ \boldsymbol{\kappa}\\ \boldsymbol{\tau}\\ e\end{bmatrix}.\tag{19}$$

Note that the representation (19) suggests that the stresses $\boldsymbol{\sigma},\boldsymbol{m},\boldsymbol{\lambda}$ and s are decoupled on the constitutive level if linear elastic microstretch materials are considered (a weak coupling exists however through the kinematic relations (7)). Moreover, $\mathbb{T}_{\mathrm{e}}$ can in its form (19) immediately be used to implement the material behavior of elastic microstretch continua into a finite element program.

3 Discretization

To make the equations derived in the previous sections accessible to a numerical treatment, their spatial discretization in the spirit of the finite element method (FEM, cf. e.g. [3,4,33,41,50] for details) is briefly presented.

As always, the material volume $\mathcal{V}$ is spatially discretized by choosing an appropriate triangulation: a collection of nodes is placed into $\mathcal{V}$ forming a grid consisting of the so-called elements $\mathcal{V}_e, e=1,\dots,n_{el}$, which satisfy

$$\begin{aligned}\mathcal{V}&=\bigcup_{e=1}^{n_{el}}\mathcal{V}_e,\\ \mathcal{V}_i\cap\mathcal{V}_{\mathbf{i}}&=\begin{cases}\partial\mathcal{V}_i\cap\partial\mathcal{V}_j & \text{if elements } i\neq j \text{ are neighbors,}\\ \emptyset & \text{otherwise}\end{cases}\end{aligned}\tag{20}$$

for $i,j\in\{1,\dots,n_{el}\}$. In two dimensions, the elements $\mathcal{V}_e$ are typically given by (sufficiently regular) triangles or rectangles, respectively. In later applications, we will decompose $\mathcal{V}$ into a varying number n_{el} of four-noded so-called $Q1$-elements.

On the element $\mathcal{V}_e$, the primary unknowns $\boldsymbol{u},\boldsymbol{\omega}$ and ξ are approximated by their discrete counterparts $\boldsymbol{u}_e^h,\boldsymbol{\omega}_e^h,\xi_e^h$ given by

$$\begin{aligned}\boldsymbol{u}_e^h&=\textstyle\sum_{k=1}^{n_{en}}\boldsymbol{u}_kN^k(\boldsymbol{x}),\quad \boldsymbol{\omega}_e^h=\sum_{k=1}^{n_{en}}\boldsymbol{\omega}_kN^k(\boldsymbol{x}),\\ \xi_e^h&=\textstyle\sum_{k=1}^{n_{en}}\xi_kN^k(\boldsymbol{x})\,,\quad e=1,\dots,n_{el}\,.\end{aligned}\tag{21}$$

Above, n_{en} denotes the number of element nodes (here, $n_{en}=4$), $N^k,k=1,\dots,n_{en}$ are the so-called shape functions and the vectors $\boldsymbol{u}_k,\boldsymbol{\omega}_k$ and ξ_k are referred to as nodal values. Note that convergence of the approximate solution to the exact one, e.g. $\boldsymbol{u}_e^h\to\boldsymbol{u}$, can in principle be achieved by either increasing n_{en} ("p-FEM") of by refining the mesh, i.e. increasing n_{el} ("h-FEM"), see [41].

A characteristic feature of the FEM is that numerical solutions for a given boundary value problem are sought starting not from its local form [here given by (9)–(12)] but taking its corresponding weak form as the point of departure, viz:

$$\begin{aligned}&\int_{\mathcal{V}}\big[\boldsymbol{\sigma}^{\mathsf{t}}+s\boldsymbol{I}\big]:\nabla_{\boldsymbol{x}}\delta\boldsymbol{u}\,\mathrm{d}v\\ &\quad=\int_{\mathcal{V}}\rho\boldsymbol{f}_{\boldsymbol{u}}\cdot\delta\boldsymbol{u}\,\mathrm{d}v+\int_{\partial\mathcal{V}}\boldsymbol{t}_{\boldsymbol{u}}\cdot\delta\boldsymbol{u}\,\mathrm{d}a\,,\\ &\int_{\mathcal{V}}\big[\boldsymbol{\epsilon}:\boldsymbol{\sigma}^{\mathsf{t}}\cdot\delta\boldsymbol{\omega}+\boldsymbol{m}^{\mathsf{t}}:\nabla_{\boldsymbol{x}}\delta\boldsymbol{\omega}\big]\,\mathrm{d}v\end{aligned}\tag{22}$$

$$= \int_{\mathcal{V}} \rho \boldsymbol{f}_{\boldsymbol{\omega}} \cdot \delta\boldsymbol{\omega}\, \mathrm{d}v + \int_{\partial\mathcal{V}} \boldsymbol{t}_{\boldsymbol{\omega}} \cdot \delta\boldsymbol{\omega}\, \mathrm{d}a\,, \tag{23}$$

$$\int_{\mathcal{V}} -\left[s\delta\xi + \boldsymbol{\lambda} \cdot \delta\nabla_{\boldsymbol{x}}\xi\right] \mathrm{d}v = \int_{\mathcal{V}} \rho f_{\xi}\delta\xi\, \mathrm{d}v + \int_{\partial\mathcal{V}} t_{\xi}\delta\xi\, \mathrm{d}a\,. \tag{24}$$

Applying the isoparametric concept, the discrete counterparts of (22)–(24) are obtained by using the relation

$$\int_{\mathcal{V}} (\bullet)\mathrm{d}v = \bigcup_{e=1}^{n_{el}} \int_{\mathcal{V}_e} (\bullet)\, \mathrm{d}v = \bigcup_{e=1}^{n_{el}} \int_{\mathcal{V}_\square} (\bullet) \det J_e^{\mathrm{iso}}\, \mathrm{d}\boldsymbol{\xi}, \tag{25}$$

stating that the sum of integrals over individual elements $\mathcal{V}_e$ can in essence be evaluated on a so-called master-element $\mathcal{V}_\square$ with local coordinates $\boldsymbol{\xi}$ [in 2d, $\mathcal{V}_\square$ is typically given by the square $[-1;1]\times[-1;1]$ so that $\boldsymbol{\xi} = (\xi_1, \xi_2)$], once $\mathcal{V}_e$ has been mapped onto $\mathcal{V}_\square$ by means of the isoparametric mapping, denoted here only by its Jacobian $\det J_e^{\mathrm{iso}}$. The discrete virtual work expression is then derived with (25) and (21) as

$$\begin{aligned}
&\bigcup_{e=1}^{n_{el}} \sum_{k=1}^{n_{en}} \delta\boldsymbol{u}_k \cdot \int_{\mathcal{V}_\square} [\boldsymbol{\sigma}^{\mathrm{t}} + s\boldsymbol{I}] \cdot \nabla_{\boldsymbol{x}} N^k \det J_e^{\mathrm{iso}} \mathrm{d}\boldsymbol{\xi} \\
&\quad = \bigcup_{e=1}^{n_{el}} \sum_{k=1}^{n_{en}} \delta\boldsymbol{u}_k \cdot \int_{\mathcal{V}_\square} \rho N^k \boldsymbol{f}_{\boldsymbol{u}} \det J_e^{\mathrm{iso}} \mathrm{d}\boldsymbol{\xi},
\end{aligned} \tag{26}$$

$$\begin{aligned}
&\bigcup_{e=1}^{n_{el}} \sum_{k=1}^{n_{en}} \delta\boldsymbol{\omega}_k \cdot \int_{\mathcal{V}_\square} [\boldsymbol{\epsilon} : \boldsymbol{\sigma}^{\mathrm{t}} N^k + \boldsymbol{m}^{\mathrm{t}} \cdot \nabla_{\boldsymbol{x}} N^k] \det J_e^{\mathrm{iso}} \mathrm{d}\boldsymbol{\xi} \\
&\quad = \bigcup_{e=1}^{n_{el}} \sum_{k=1}^{n_{en}} \delta\boldsymbol{\omega}_k \cdot \int_{\mathcal{V}_\square} \rho N^k \boldsymbol{f}_{\boldsymbol{\omega}} \det J_e^{\mathrm{iso}} \mathrm{d}\boldsymbol{\xi},
\end{aligned} \tag{27}$$

$$\begin{aligned}
&\bigcup_{e=1}^{n_{el}} \sum_{k=1}^{n_{en}} \delta\xi_k \int_{\mathcal{V}_\square} -[sN^k + \boldsymbol{\lambda} \cdot \nabla_{\boldsymbol{x}} N^k] \det J_e^{\mathrm{iso}} \mathrm{d}\boldsymbol{\xi} \\
&\quad = \bigcup_{e=1}^{n_{el}} \sum_{k=1}^{n_{en}} \delta\xi_k \int_{\mathcal{V}_\square} \rho N^k f_{\xi} \det J_e^{\mathrm{iso}} \mathrm{d}\boldsymbol{\xi}\,.
\end{aligned}$$

Remark 5 We have neglected those entries in the discretized weak form which are due to given generalized boundary tractions, cf. (12): they can be treated in full analogy to the classical Boltzmann continuum formulations. In other words, the boundary tractions associated with the additional degrees of freedom require no special attention in coding at all.

With the help of the (element) strain–displacement operator (typically denoted by $\boldsymbol{B}_e$), the (components of) strain $\boldsymbol{\varepsilon}$, curvature $\boldsymbol{\kappa}$, stretch gradient $\boldsymbol{\tau}$ and effective dilatation e are computed on each element $\mathcal{V}_e$ for node k from the primary unknowns $\boldsymbol{u}, \boldsymbol{\omega}$ and ξ. For plane strain conditions (in the x, y-plane), to which attention is restricted in the subsequent numerical examples, the primary unknowns reduce to $\boldsymbol{u} = (u, v)$, $\boldsymbol{\omega} = \omega$ and ξ while $\boldsymbol{B}_e$ is (at each node k) given by

$$\boldsymbol{B}_{e,k} = \begin{pmatrix}
N_{k,x} & 0 & 0 & 0 \\
0 & N_{k,y} & 0 & 0 \\
0 & 0 & 0 & 0 \\
N_{k,y} & 0 & N_k & 0 \\
0 & N_{k,x} & -N_k & 0 \\
0 & 0 & N_{k,x} & 0 \\
0 & 0 & N_{k,y} & 0 \\
0 & 0 & 0 & N_{k,x} \\
0 & 0 & 0 & N_{k,y} \\
N_{k,x} & N_{k,y} & 0 & -N_k
\end{pmatrix}. \tag{28}$$

In (28), $N_{k,(\cdot)}$ denotes differentiation of N_k with respect to $(\cdot)$ and we have used the fact that the discrete analogs of the strain $\boldsymbol{\varepsilon}$, the curvature $\boldsymbol{\kappa} = \nabla_{\boldsymbol{x}}\boldsymbol{\omega}$, the stretch gradient $\boldsymbol{\tau} = \nabla_{\boldsymbol{x}}\xi$ and the effective dilatation $e = \nabla_{\boldsymbol{x}}\boldsymbol{u} : \boldsymbol{I} - \xi$ are given by [cf. (7) and (21)]

$$\begin{aligned}
\boldsymbol{\varepsilon}_e^h &= \textstyle\sum_{k=1}^{n_{en}} \boldsymbol{u}_k \otimes \nabla_{\boldsymbol{x}} N^k(\boldsymbol{x}) + \sum_{k=1}^{n_{en}} \boldsymbol{\epsilon} \cdot \boldsymbol{\omega}_k N^k(\boldsymbol{x}), \\
\boldsymbol{\kappa}_e^h &= \textstyle\sum_{k=1}^{n_{en}} \boldsymbol{\omega}_k \otimes \nabla_{\boldsymbol{x}} N^k(\boldsymbol{x}), \\
\boldsymbol{\tau}_e^h &= \textstyle\sum_{k=1}^{n_{en}} \xi_h \nabla_{\boldsymbol{x}} N^k(\boldsymbol{x}), \\
e_e^h &= \textstyle\sum_{k=1}^{n_{en}} \boldsymbol{u}_k \otimes \nabla_{\boldsymbol{x}} N^k(\boldsymbol{x}) : \boldsymbol{I} - \sum_{k=1}^{n_{en}} \xi_k N^k(\boldsymbol{x}).
\end{aligned} \tag{29}$$

Again, the argumentation used to combine the discrete strain-displacement operator $\boldsymbol{B}_{e,k}$ and the elasticity matrix $\mathbb{T}_{\mathrm{e}}$ from (19) to form the element stiffness matrix is of the standard form found in simple linear elasticity involving the typical multiplication $\boldsymbol{B}_e^T \mathbb{T}_{\mathrm{e}} \boldsymbol{B}_e$. The same holds true when computing the internal force vector.

Remark 6 The plane strain condition that will be imposed in all forthcoming numerical examples is $\varepsilon_{33} = 0$ as is well-known when dealing with Boltzmann continuum formulations. However, for a continuum with additional internal degrees of freedom giving eventually rise to additional strain measures, cf. (7), it is not a priori obvious how a plane strain conditions has to be formulated. Here, we have chosen to leave the second naturally arising strain measure, namely the effective dilatation e, unrestricted: this implies that neither the stretch ξ nor the rotation ω affect the plane condition. Furthermore, the particular choice of the plane strain condition utilized is the one which can be most accurately approximated when performing experiments to identify real material parameters in a further project stage; it is not clear to the authors how to keep track of a plane strain condition involving the non-standard degrees of freedom, thus the choice of the condition is the only appropriate one.

4 Numerical examples

4.1 General remarks

To motivate our numerical investigations, we recall that in the numerical modeling of the behavior of e.g. strain softening materials, the independent rotational degree of freedom introduced in polar continuum formulations as an amendment to the standard Boltzmann continuum has a regularizing effect. The latter is to be understood in the sense that the pathological mesh dependence of the post-peak response (which is observed for implementations based on the standard continuum formulation) is overcome, cf. Sect. 1 and the references listed there. While the independent rotational degree of freedom is obviously activated under shearing loads, it is certainly inactive when tensile loads are applied—consequently, numerical schemes based on the polar theory for problems dominated by the application of tensile loads can in general not be expected to benefit from the regularizing effect of the independent rotational degree of freedom. To cure this drawback, we have thus introduced an additional independent stretching degree of freedom, cf. Sect. 2, which is in particular activated under tensile and compressive loads. In other words, it is hoped that by generalizing the polar theory to microstretch theory numerical computations for e.g. strain softening elastoplastic microstretch materials turn out to be mesh-independent irrespective of whether shear loads or tensile/compressive loads are applied.

As the treatment of localization phenomena in inelastic microstretch continua can be viewed as a long-term goal, we will here study the effects of the additional stretching degree of freedom designed to capture microstructural properties as well as its influence on typical macroscopic quantities for (hyper)elastic materials only. In particular, it has to be shown that the numerical routines developed for the microstretch continuum exhibit a downward-compatibility in the sense that micropolar material behavior is recovered by switching of all stretch-related effects. Further, we expect to detect possible mutual interaction between the Cosserat rotational degree of freedom and the stretching degree of freedom by comparing a restricted[4] microstretch model (in which independent rotations are neglected) and a full microstretch model. For notational convenience, we thus introduce the following nomenclature for the three different models investigated in the sequel (degrees of freedom is abbreviated by dof):

- case ①: polar model;
  displacement field $\boldsymbol{u}$ + Cosserat rotations $\boldsymbol{\omega}$ (6 dof in 3d/3 dof in 2d)
- case ② restricted microstretch model;
  displacement field $\boldsymbol{u}$ + independent isotropic stretch ξ (4 dof in 3d/3 dof in 2d);
- case ③ full microstretch model;
  displacement field $\boldsymbol{u}$ + Cosserat rotations $\boldsymbol{\omega}$ + independent isotropic stretch (7 dof in 3d/4 dof in 2d).

4.2 Prelude: referential "volume" element subject to simple shear

In the first numerical example, a two-dimensional referential "volume" element exhibiting elastic microstretch material behavior is subjected to simple shear while plane strain conditions are prescribed. We wish to show that the rotational degree of freedom ω is—as expected—activated while the stretching degree of freedom, ξ, remains inactive.

Consequently, the set of nodal degrees of freedom is given by $\{u, v, \omega, \xi\}$, where u and v are the horizontal and vertical macroscopic displacement (i.e. the displacements in x and y-direction), ω is the rotation about the normal (i.e. the z-axis) to the xy-plane, and ξ is the isotropic stretch acting uniformly in the x and y direction. In its undeformed state, the specimen has a size of 6 cm by 6 cm and is discretized by 24 quadrilateral, four-noded elements ($Q1$ elements). However, the authors are aware of the drawbacks of a simple Q1-element formulation which leads by the particular definition of the strain measures in (7) to different, incomplete polynomial approximations of the various strains; the easiest way to cure this drawback is the implementation of the material model in a Taylor–Hood-type framework with complete monomials to approximate the macro- and microscopic strains. Furthermore, this will also to increase the speed of spatial convergence; the implementation is scheduled for the next step.

A total horizontal displacement of 0.3 cm is prescribed at the top boundary of the specimen, giving rise to a global strain of 5%. The material parameters used in the numerical simulations are given by

$$K_\xi = 1 \quad \text{GPa}, \quad \mu_c = 5.77\,\text{GPa}, \qquad l = 0.5\,\text{mm}, \quad \pi_\xi = 5\,\frac{\text{kN}}{\text{mm}}, \tag{30}$$

and

$$K = 25\,\text{GPa}, \quad \mu = 11.54\,\text{GPa}\,. \tag{31}$$

[4] To date, a universally accepted terminology for this material, which is referred to as "dilating continua of Goodman–Cowin type" in [44], is not yet available.

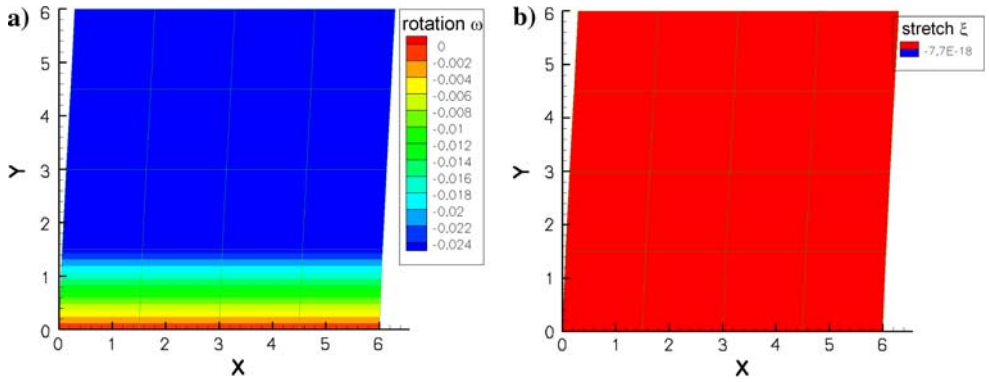

Fig. 1 Distribution of **a** independent rotation and **b** stretch in a referential 2d region subject to simple shear, cf. Sect. 4.2, as obtained for model ③

Remark 7 Note that the bulk modulus K and the shear modulus μ are determined via prescribing Young's modulus E and Poisson's ratio ν as $E = 30,000$ MPa and $\nu = 0.3$ according to the formulae

$$K = \frac{E}{3(1-2\nu)}, \quad \mu = \frac{E}{2(1+\nu)}, \tag{32}$$

while μ_c is chosen as 0.5μ.

Prescribing boundary conditions such that $\omega = 0$ holds at the bottom nodes of the specimen, the following results are obtained for the full microstretch model ③: The absolute value of the rotation ω increases from its (prescribed) minimum $\omega = 0$ at the bottom to $|\omega| = 0.024$ at the top of the specimen, while the stretch ξ is zero everywhere, cf. Fig. 1. Note that a relaxation of the boundary conditions imposed on ω (i.e. leaving ω unconstrained at the bottom) results in a homogeneous distribution of independent rotation, $\omega = -0.024$, throughout the specimen. The negative sign corresponds to a shearing in positive x-direction; the sign changes if a horizontal displacement in negative x-direction is prescribed. Obviously, the full microstretch model ③ behaves as expected in simple shear tests – we are thus encouraged to proceed with the investigation of (the hierarchy of) models ①–③ in tensile tests; this is the subject of the following subsections.

4.3 Non-contracting strip subjected to uniaxial tension

In this second example, a twodimensional strip exhibiting elastic microstretch material behavior is subjected to a uniform tensile load while, again, plane strain conditions are prescribed. Prior to deformation, the strip has an initial length of 2 cm, while its width is chosen as 1 cm. The strip is discretized by 32 $Q1$-elements and the tensile load acting at the top of the strip is modeled by prescribing a total displacement of 0.1 cm; hence, the applied axial global strain amounts to 5%. The material parameters are as given in (30), (31). Prescribing boundary conditions, the bottom nodes at $y = 0$ are fixed in the sense that a macroscopic displacement in horizontal as well as vertical direction is prohibited (i.e. $u|_{y=0} = v|_{y=0} = 0$), while the microscopic degrees of freedom (rotation and stretch) have no preassigned values at $y = 0$ and remain thus unconstrained. Moreover, to avoid transverse contractions of the specimen, also the nodes at $y = \text{const}$-gridlines are constrained in x-direction: $u|_{y=\text{const}} = 0$. These particular constraints will be removed later on to allow for the investigation of the onset of necking phenomena.

Next we consider the results obtained for the model hierarchy ①–③: As expected, we observe non-activated and hence vanishing independent rotations in the Cosserat-model ①, cf. Fig. 2a. Turning attention to the restricted microstretch model ②, we observe the development of a non-vanishing uniform stretch-field with $\xi = 0.005$, cf. Fig. 2b. As the stretch is uniform, its

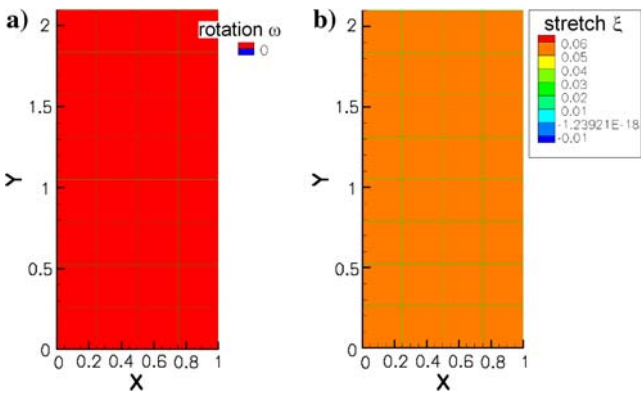

Fig. 2 Distribution of rotation **a** and stretch **b** in a non-contracting strip subject to uniaxial tension, cf. Sect. 4.3. The rotations are plotted for model ①, while the stretch distribution results from model ②. The microscopic degrees of freedom are unconstrained at the bottom boundary

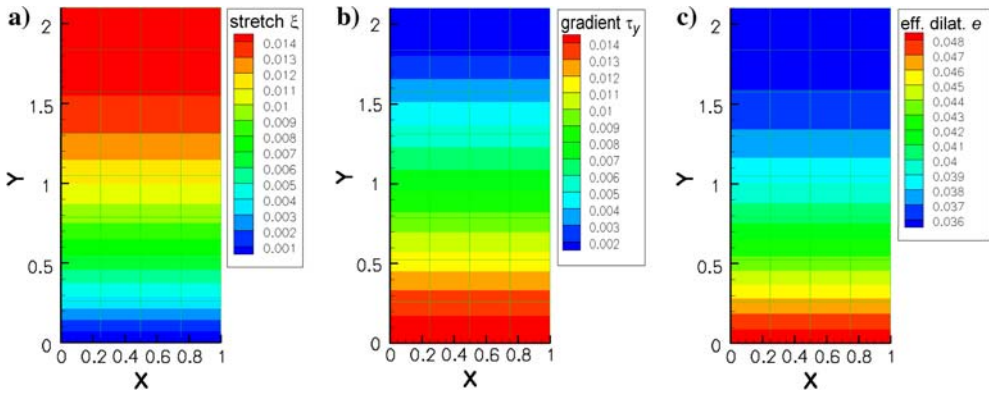

Fig. 3 Distribution of **a** stretch ξ, **b** vertical stretch gradient τ_y and **c** effective dilatation e in a non-contracting strip subject to uniaxial tension, cf. Sect. 4.3. Results are plotted for model ②, and $\xi|_{y=0} = 0$ is prescribed as boundary condition

value adjusts itself [due to energy considerations, cf. (15)] such that the effective dilation e vanishes and hence does not contribute to the stored energy W. Then, by virtue of (19), also the microstretch pressure s vanishes, $s = 0$. Finally, as $\boldsymbol{\tau} = \nabla\xi$, the stretch gradient vanishes by definition. For the particular set-up chosen for this first numerical example (tensile loaded non-contracting specimen), we expect no changes of the so-far obtained numerical results when turning to the full microstretch model ③: as the Cosserat rotations are not activated, they can not interfere with the microstretch degree of freedom. Hence, the distribution of rotation and of stretch are exactly as in Fig. 2. They are not reproduced here and lead, as for model ②, to vanishing microstress $\boldsymbol{\tau}$, microstretch pressure s and effective dilatation e.

Remark 8 It is mentioned that the axial stress σ_{yy} assumes a constant value of $\sigma_{yy} = 2020$ MPa for all models ①–③.

Let us now consider a slightly different situation in which only the boundary conditions for ω and ξ are modified: for the setting described above, we now constrain the microstructural degrees of freedom at the bottom of the strip such that $\omega|_{y=0} = 0$ and/or $\xi|_{y=0} = 0$ at the respective nodes holds. The results are as follows: as the rotations are not activated under tensile loads, the boundary condition on ω has no effects in the polar model ①. Consequently, we have again vanishing rotations. The restricted microstretch model ② however is influenced by fixing the stretch ξ to zero at the bottom of the strip: a stretch field that is varying with y develops and attains its maximal value $\xi = 0.014$ for $y = 2.1$ and all $x \in [0; 1]$, see Fig. 3a. As ξ does not vary with x, only the y-component of the stretch gradient $\boldsymbol{\tau} = (\tau_x, \tau_y)$ is non-vanishing: τ_y assumes values in $[0.002; 0.014]$ and is strongest developed in a bottom boundary layer, see Fig. 3b. Overall, the specimen is dominated by the macroscopic material response as the effective dilatation e has positive values in the entire strip. Since the maximum values of e are localized close to the bottom of the strip and decrease toward its top, micro- and macroscale material behavior is recognized to be pronounced different from each other in this bottom boundary layer while it is becoming less disparate toward the top, see Fig. 3c. The stress(like) quantities corresponding to the (y component of the) stretch gradient and the effective dilatation are the (y component of the) microstress vector $\boldsymbol{\lambda}$ and the microstretch pressure s: both are displayed in Fig. 4a and b. In contrast to the homogeneous distribution of the macroscopic axial stress σ_{yy} (which again assumes a constant value of $\sigma_{yy} = 2020$ MPa for models ①–③, cf. Remark 8), the microscopic stresses λ_y and s vary significantly with y, albeit their nominal values are two orders of magnitude smaller than the macroscopic axial stress. Turning to the full microstretch model

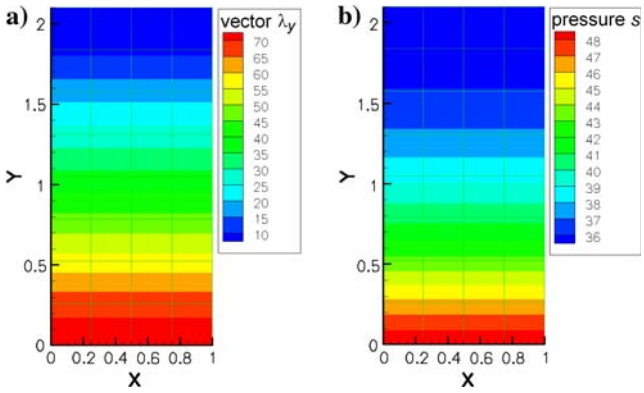

Fig. 4 Distribution of the vertical component of the microstretch vector λ_y **a** and the microstretch pressure s **b** in a non-contracting strip subject to uniaxial tension, cf. Sect. 4.3. Results are plotted as obtained from model ② , and $\xi|_{y=0} = 0$ is imposed as a boundary condition

③, the numerical simulations reproduce—as expected—exactly those obtained for model ② and are hence not re-displayed.

4.4 Horizontally contracting strip subjected to uniaxial tension

In the following, a horizontal contraction of the linearly elastically behaving microstretch strip will be accounted for. This is achieved by relaxing, in the interior[5] of the strip, the constraints imposed beforehand (in Sect. 4.3) on nodal degrees freedom in x-direction: we no longer require $u|_{y=\text{const}} = 0$ but rather let $u|_{y=\text{const}}$ unconstrained. Although the macroscopic contraction is almost negligible due to the small overall deformation of only 5%, it can certainly be regarded as the onset of necking. Moreover, it is powerful enough to trigger microscopic effects: first, the rotational degree of freedom, ω, is activated in regions where horizontal contractions (however small they may be) occur. Consequently, the two additional microstructural degrees of freedom, stretch and rotation, are now competing and their individual influence on the material response has to be determined. Moreover, a non-uniform distribution of stretch is obtained even for unconstrained stretch boundary conditions as will be seen in Sect. 4.4.2.

Remark 9 As in the preceding examples, we shall investigate linearly elastic microstretch material behavior subject to two different types of boundary conditions given either by $\xi|_{y=0} = 0$ (cf. Sect. 4.4.1) or by letting $\xi|_{y=0}$ unconstrained (cf. Sect. 4.4.2). It is remarked that we refrain from varying the boundary conditions for the independent rotations (ω is free to develop as no boundary condition is imposed) since the primary focus is on the distribution of stretch ξ.

4.4.1 Constrained stretch boundary conditions

We now apply a tensile load resulting in an axial global strain of 5% at both ends of the strip introduced in Sect. 4.3. The boundary conditions for the stretch field are prescribed such that $\xi|_{y=0} = 0$ and $\xi|_{y=2} = 0$, that is, the stretch is forced to vanish at the top and bottom nodes of the specimen. The material parameters remain unchanged and are listed in (30) and (31). Prior to the presentation of numerical results, we emphasize the role of the material parameters:

Remark 10 Judging from (15) alone, the parameters K_ξ, μ_c, l and π_ξ can in principle take any values in $\mathbb{R}^+$—physically meaningful ranges are only known for the bulk modulus K and the shear modulus μ. Thus, a detailed parameter study revealing the influence and likely range of K_ξ, π_ξ, μ_c and l is certainly one of the pressing issues to be addressed in the modeling of microstretch continua. However, doing this at an untimely stage (i.e., too early) we would (with the words of the statistician J. Naisbitt) be "drowning in information and starving for knowledge". In all here presented numerical examples, we have hence fixed the material parameters to the values given in (30) and (31). In addition, we have performed a first parameter screening the outcome of which suggests that the parameters K_ξ, π_ξ, μ_c and l act like penalty parameters as occurring e.g. in the (algorithmic) treatment of contact mechanics: Large values of l and μ_c (whereby "large" means "large in comparison to K_ξ and π_ξ and has still to be quantified) severely limit the influence of $\boldsymbol{\kappa} = \nabla\boldsymbol{\omega}$ and $\mathsf{spn}\boldsymbol{\omega}$ in the minimization of Π or ψ, respectively. Consequently, large l and large μ_c imply that effects due to the independent rotational field $\boldsymbol{\omega}$ are suppressed, enabling the microstretch related effects to dominate the scene. Vice versa, large values of K_ξ and π_ξ penalize the stretch-related contributions and allow a pronounced development of Cosserat-effects in a full microstretch model.

The parameter screening addressed in Remark 10 indicates that K_ξ, π_ξ as given in (30) are "large" penalties while l and μ_c are "small". Thus, in the mutual interaction of ω and ξ in the full microstretch model ③, the stretch-related effects will be dominated by strongly developed rotational effects. For the here considered horizontally contracting strip, we have chosen to present only numerical results obtained for model ③: a comparison of models ①, ② and ③ is postponed to Sect. 4.5 where a modified geometry (enhanced by a notch) favors the development of differences in the numerical results.

Starting with the primary macroscopic and microscopic quantities, we plotted in Fig. 5a and b the macroscopic horizontal and vertical displacement u and v, respectively, and the fields of independent rotation ω and stretch ξ, views c and d in Fig. 5. The horizontal contraction manifests itself in the distribution of u, cf. Fig. 5a, and the slight arching of the isolines in the distribution of v is attributed to the boundary conditions, see Fig. 5b. The rotations are antisymmetric about both symmetry axes (at $x = 0.5$ and $y = 1$) and are activated under the applied tensile load solely because the material has (due to the relaxed conditions on $u|_{y=\text{const}}$) gained an additional mobility, cf. Fig. 5c. In Fig. 5d, a pronounced variation in the stretch field is observed: from the loaded boundaries, where the boundary conditions enforce $\xi = 0$, the values of the stretch increase to reach

[5] That is, everywhere except at the bottom and the top.

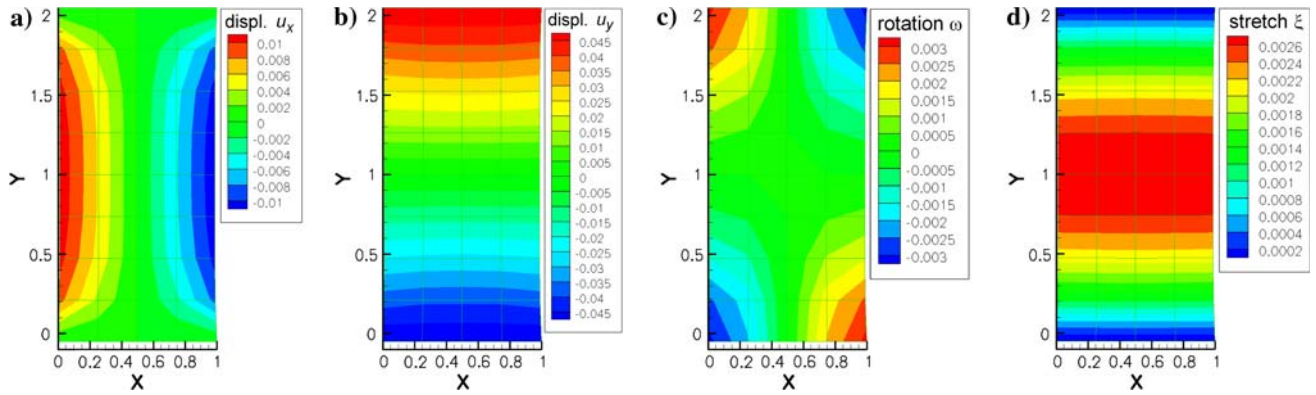

Fig. 5 Horizontal and vertical displacement **a** and **b**, rotation **c** and stretch **d** for a horizontally contracting strip subject to uniaxial tension, cf. Subsect. 4.4. Results are plotted for model ③, and $\xi|_{y=0} = \xi|_{y=2} = 0$ has been imposed as boundary condition

a maximal value of $\xi = 0.0026$ in the central region of the strip. Yet the stretch effects are small compared to the overall macroscopic response in volumetric strain as captured by $\nabla \boldsymbol{u} : \boldsymbol{I}$: the effective dilation $e = \boldsymbol{u} : \boldsymbol{I} - \xi$ is with $e \in [0.027, 0.042]$ positive throughout the specimen. The distribution of e as shown in Fig. 6a however suggests that micro- and macroscale effects captured by $\nabla \boldsymbol{u} : \boldsymbol{I}$ and ξ, respectively, are almost equally influential in an hourglass-like region formed by minimal values of e and located in the central region of the strip experiencing the largest horizontal contractions. Finally, we present in Fig. 6b the x-component of the microstretch vector, λ_x. It is, for the linearly elastic material behavior considered here, proportional to the x component of the stretch gradient, τ_x, via (19). It is observed that λ_x, and hence τ_x, is symmetric about both axis of symmetry and assumes its largest values for those y where, at $x = 0$ and $x = 1$, maximal changes in horizontal displacements are detected.

4.4.2 Unconstrained stretch boundary conditions

Relaxing the boundary conditions imposed on the stretching degree of freedom in Sect. 4.4.1, we now let ξ be unconstrained while the remainder of the set-up is unchanged. The interesting results are the distribution of stretch and effective dilatation—all other quantities remain either more or less unchanged or are (in the linearly elastic regime) directly related to ξ and e.

The distribution of the stretch field as obtained from model ③ is plotted in Fig. 7a. Recall that in the preceding examples, unconstrained stretch values at the boundaries necessarily implied the development of a uniform stretch field in the specimen. However, in the present example, where horizontal contraction of the specimen is allowed, a non-uniform stretch field develops although the stretch values at $y = 0$ and $y = 2$ are unconstrained. We note that the resulting stretch field (although positive in the entire specimen as was the case

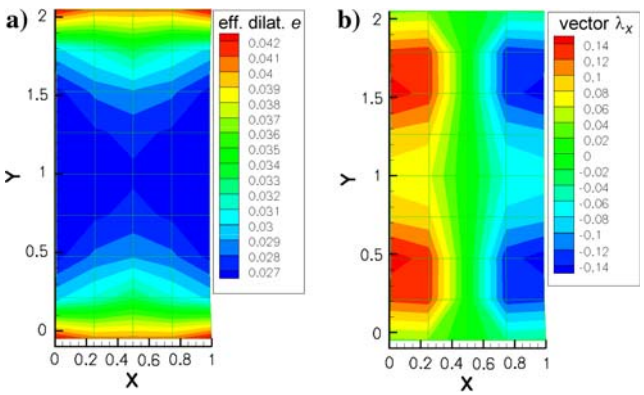

Fig. 6 Distribution of effective dilatation e **a** and the x-component of the microstretch vector, λ_x **b** for a horizontally contracting strip subject to uniaxial tension, cf. Subsect. 4.4. Results are plotted for model ③, and $\xi|_{y=0} = \xi|_{y=2} = 0$ has been imposed as boundary condition

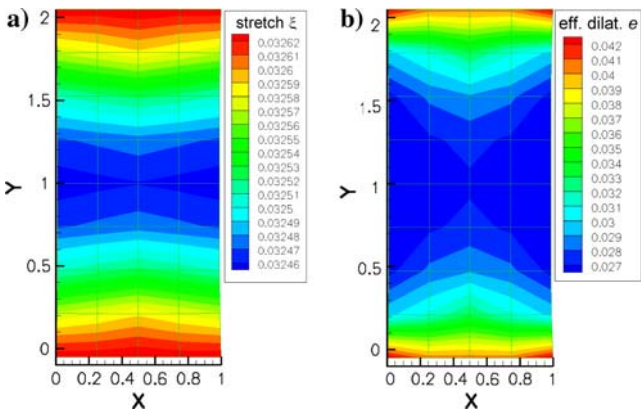

Fig. 7 Distribution of stretch ξ **a** and effective dilatation e **b** in a horizontally contracting strip subject to uniaxial tension, cf. Sect. 4.4. Results are plotted for model ③, and the stretch ξ is unconstrained at the boundaries

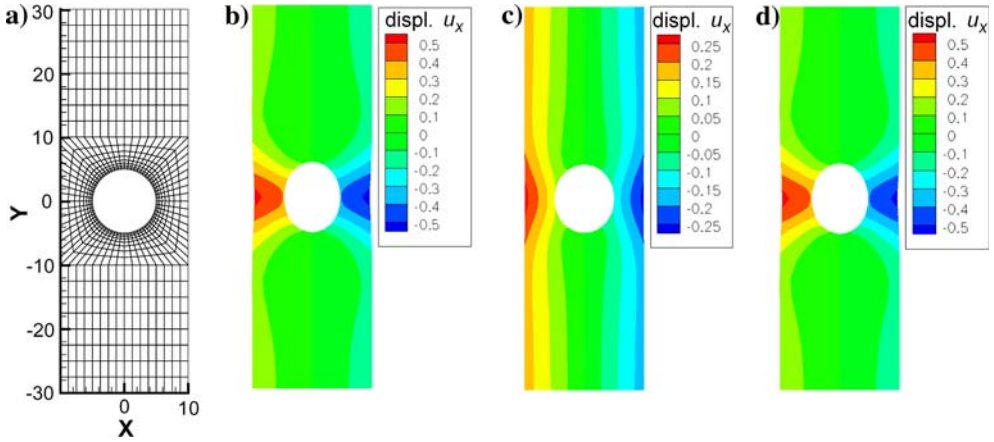

Fig. 8 A horizontally contracting, notched strip subject to uniaxial tension is meshed by 768 $Q1$ elements **a**, cf. Sect. 4.5. For brevity, the mesh and the axes are omitted when the horizontal displacement u is plotted for models ①–③ in panels b–d

in Sect. 4.4.1) is different from the one obtained if restrictions are imposed on $\xi|_{y=0}$ and $\xi|_{y=2}$. As a matter of fact, with increasing distance from $y = 1$, that is for $y \to 2.05$ and $y \to -0.05$, the values of ξ increase but it is emphasized that the variation in the stretch takes place at a small scale only: the difference between minimal and maximal values amounts only to 0.00016. Moreover, it is recognized that even the "large" stretch values at the ends of the strip are small compared to the macroscopic values of $\nabla \boldsymbol{u} : \boldsymbol{I}$ as the effective dilatation e is positive at the bottom and the top of the strip, cf. Figure 7.b. It is in the interior of the strip where, despite "small" stretch values, microscopic effects dominate over the macroscopic contribution $\nabla \boldsymbol{u} : \boldsymbol{I}$ as $e < 0$. This behavior is fundamentally different (despite plots looking almost alike, cf. also Figure 6.a from the one observed for the effective dilatation e (which in the present example has values in $[-0.002; 0.01]$) if ξ is constrained at the top and bottom boundaries of the specimen.

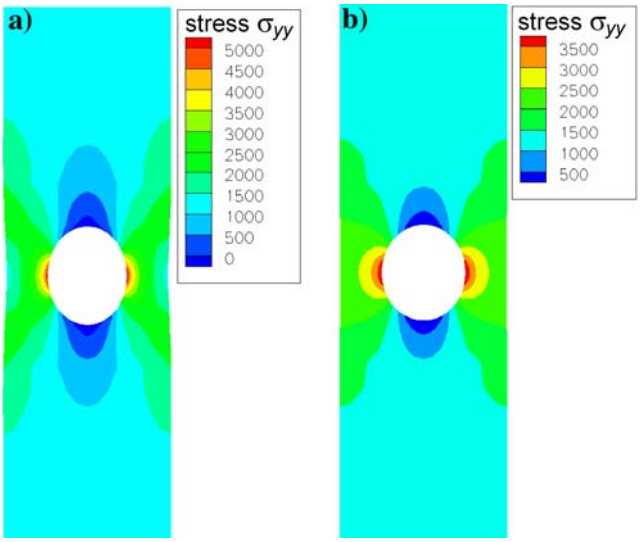

Fig. 9 Distribution of axial stress σ_{yy} in a horizontally contracting, notched strip in tension, cf. Sect. 4.5. Identical results are obtained for models ① and ③, cf. panel a, while those for model ② shown in panel b differ. The well-known stress concentration by a factor 3 is reproduced in all models

4.5 Horizontally contracting, notched strip subjected to uniaxial tension

In the following, a twodimensional, horizontally contracting notched strip consisting of elastic microstretch material is investigated. Initially, the strip has a length of 6 cm in the y direction and a width of 2 cm in the x direction. A mesh consisting of 768 $Q1$ elements is used, cf. Fig. 8a, and a global axial strain of 5% (elongating the strip to 6.3 cm) is applied. As before, the material parameters are taken from (30) and (31). Note that in order to facilitate the plot-reading, the mesh as well as the axes are omitted in all forthcoming figures. For brevity,[6] we present only numerical results for unconstrained microscopic boundary conditions, i.e. no values are preassigned to $\xi|_{|y|=30}$ and $\omega|_{|y|=30}$. Again, this choice of boundary condition is motivated by experimental capabilities which allow to control macroscopic displacements but no additional degrees of freedom such as rotations or stretch; furthermore, no difficulties

[6] Prescribing $\xi|_{|y|=30} = 0$ merely forces the stretch values to decrease to zero within a thin boundary layer. The far field values of ξ, i.e. the distribution of stretch away from the bottom and top boundary layer, is not affected by the boundary conditions imposed on ξ.

in obtaining unique numerical results were detected even without prescribing a single value of the fields. Macroscopically, the strip is fixed at its bottom boundary to resist a vertical motion so that $v|_{y=-30} = 0$. Note that a horizontal contraction of the specimen can take place as no conditions on u are imposed.

Investigating this typical, often benchmarked geometry, numerical results obtained for the polar, the restricted and the full microstretch model are presented now in a synoptical manner in order to demonstrate the penalizing effect of the material parameters arising in (15), cf. Remark 10. Starting with macroscopically observable quantities, we first present the horizontal displacement as obtained for models ①–③ in Figs. 8b–d. For the polar model ①, the distribution of horizontal displacement is antisymmetric about the axis $x = 0$ and symmetric about the axis $y = 0$, cf. Fig. 8b, and has non-vanishing values in a horizontal layer the length (in y direction) of which encompasses en gros the notch. These nonvanishing values of u visualize the horizontal contraction which is, however, so small that it is hardly visible in unscaled plots. Comparing the results for u for the polar model with those obtained for the full microstretch model ③, no differences can be detected, cf. Fig. 8d. This indicates that K_ξ and π_ξ have been assigned values which are large in comparison to μ_c and l and that the former penalize the stretch contributions, cf. Remark 10. If the rotations are omitted as in the restricted microstretch model ②, the distribution of horizontal displacement is qualitatively and quantitatively different from the one obtained for models ① and ③, see Fig. 8c. While the axes of symmetry remain unchanged compared to models ① and ③, the action of the microstretch ξ in model ② gives rise to a pronounced vertically banded distribution of horizontal displacement throughout the entire strip. It is emphasized that the overall horizontal contraction is smaller (by a factor 2) than in models ① and ③. Comparing the restricted and the full microstretch model, we observe that non-negligible interferences between the stretching degree of freedom and the rotational degree of freedom develop: the responsible agent for this are small values of l and μ_c which penalize contributions stemming from ω only to a very small extend. Numerical results obtained for the vertical displacement y exhibit exactly the same features as just presented for the horizontal displacement: models ① and ③ yield identical distributions of y, while it is slightly different for model ②—for brevity, corresponding plots are not shown.

Among the macroscopic quantities, we rather present the results obtained for the axial stress σ_{yy} in Fig. 9a (results obtained for models ① and ③) and b (results obtained for model ②). As above, the full microstretch model ③ is – due to the choice of material parameters – dominated by the action of the independent rotation, which is why models ① and ③ yield identical results, cf. also Remark 10. Note, however, that the well-known stress–concentration by a factor 3 at those edges of the notch pointing toward the lateral boundaries of the strip is reproduced in all models. Turning to the microscopic quantities ω and ξ, the plots in Fig. 10 are consistent with the preceding ones in the sense that they confirm the interpretation of the parameters as discussed above: The rotations are the same in models ① and ③—in other words, the rotations are in a full microstretch model not affected at all by the presence of the additional stretching degree of freedom, cf. Fig. 10a. We refrain from plotting the rotations for model ②. In contrast, the stretch is affected by the presence of a rotational degree of freedom, indicating that ω dominates over ξ for the choice of parameters given in (30) and (31). As ξ changes from 2 to 3, differences can also be detected in the derived (e and $\boldsymbol{\tau}$) and conjugated (s and $\boldsymbol{\lambda}$) quantities, but corresponding plots are not shown for the sake of brevity.

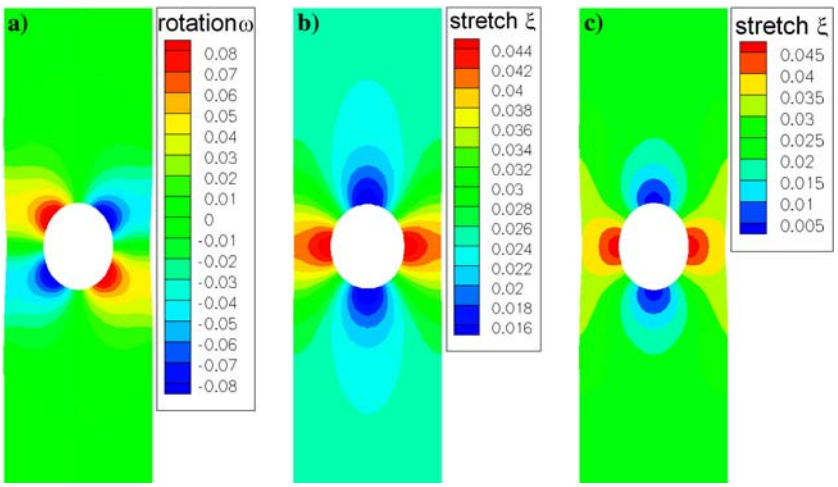

Fig. 10 **a** Distribution of rotation in a horizontally contracting, notched strip in tension, cf. Sect. 4.5. Identical results are obtained for models ① and ③. **b**, **c** Distribution of stretch in a horizontally contracting, notched strip in tension, cf. Sect. 4.5. Different results are obtained for models ② and ③, cf. **b** and **c**

5 Conclusion and outlook

The investigation of microstretch and micromorphic continua (which are prominent examples of so-called extended continua) dates back to Eringens pioneering works in the mid 1960ies, cf. [12,14,18]. Despite the fact that 40 years have passed, and despite the fact that many of todays innovative engineering materials are characterized by an inherent microstructure calling for extended continuum modeling approaches, micromorphic and microstretch continuum theories have not gained a broad acceptance in engineering. Consequently, numerical investigations for micromorphic materials are rare.

To overcome this drawback, first numerical benchmarks for microstretch continua in engineering applications have been established in this article. The numerical implementation of the model equations by means of the finite element method is conceptually straightforward if the governing equations of microstretch continua are derived in a variational framework as given by the application of Dirichlet's principle—this procedure has been presented here, cf. Sect. 2, and complements Eringens approach in a novel way.

Upon postulating a specific expression for the Helmholtz free energy, Eringens balance equations have been re-derived, and constitutive relations describing elastic microstretch material behavior were obtained as a "by-product" of the variational analysis, cf. Sect. 2. It has also been shown that the microstretch model derived here exhibits a "downward-compatibility" to Cosserat continuum models in the sense that by switching off all stretch-related effects, a polar continuum model is regained. The focus in the numerical analysis presented in Sect. 4 has thus been on a hierarchy of models, namely a full microstretch model (denoted by ③ and including Boltzmann, Cosserat and stretching degrees of freedom), a restricted microstretch model (referred to by ② and characterized by Boltzmann and stretching degrees of freedom), and the polar model (abbreviated by ① and including Boltzmann and Cosserat degrees of freedom). The specimens investigated exhibit simple, twodimensional geometries and are subjected to a plane strain condition. Numerical results have been produced for a fixed set of material parameters characterizing the free energy, while various boundary conditions prescribed for the microstructural degrees of freedom (independent rotations, stretch) have been accounted for. It has been shown that those material parameters in the free energy which are related to the additional microscopic degrees of freedom play a crucial role in the numerical analysis—they can act as penalty parameters as known e.g. in the algorithmic treatment of contact mechanics.

In order to gain more insight into the complex interaction of microstructural effects described by independent Cosserat rotations and an independent stretch field, a detailed parameter study, revealing e.g. conditions under which an equally weighted co-existence of stretch effects and Cosserat effects in the full microstretch model ③ is possible, is thus of pressing importance. Adding additional relevance to this issue, work in progress has shown that material parameters may not be chosen independently from each other—the algorithmic treatment of plasticity based on the standard radial return algorithm is only applicable if some of the material parameters are coupled.

Thus, the modeling, algorithmic treatment and numerical investigation of inelastic microstretch materials is the next step to be undertaken. Hoping for a regularizing effects of the stretching degree of freedom in tensile test (where the known regularization of the Cosserat rotations is not activated), strain softening plasticity for microstretch materials will be in the focus of a forthcoming article.

References

1. Aifantis EC (1984) On the microstructural origin of certain inelastic models. J Eng Mat Tech 106:326–330
2. Allen SJ, DeSilva CN, Kline KA (1967) Theory of simple deformable directed fluids. Phys Fluids 10(12):2551–2555
3. Braess D (2001) Finite elements. theory, fast solvers and applications in solid mechanics. Cambridge University Press, London
4. Brenner SC, Scott LR (2002) The mathematical theory of finite element methods, 2nd edn. Springer, Berlin Heidelberg New York
5. Ciarletta M (1999) On the bending of microstretch elastic plates. Int J Eng Sci 37(10):1309–1318
6. Cosserat E, Cosserat F (1909) Théorie des corps déformable. Hermann et Fils
7. Cowin SC (1974) The theory of polar fluids. Adv Appl Mech 14:279–347
8. deBorst R (1991) Simulation of strain localization: a reappraisal of the Cosserat continuum. Eng Comput 8:317–332
9. DeCicco S (2003) Stress concentration effects in microstretch elastic bodies. Int J Eng Sci 41(2):187–199
10. Diebels S (1999) A micropolar theory of porous media: constitutive modelling. Transport Porous Media 34:193–208
11. Dietsche A, Steinmann P, Willam K (1993) Micropolar elastoplasticity and its role in localization analysis. Int J Plast 9:813–831
12. Eringen AC (1966) Mechanics of micromorphic materials. In: Görtler H, Sorger P (eds) Proceedings of 11th international congress of applied mechanics Springer, Berlin Heidelberg New York, pp 131–138
13. Eringen AC (1968) Theory of micropolar elasticity. In: Liebowitz H (ed) Fracture. An advanced treatise, vol II. Academic, New York, pp 621–729
14. Eringen AC (1970) Balance laws of micromorphic mechanics. Int J Eng Sci 8:819–828

15. Eringen AC (1972) Theory of micromorphic materials with memory. Int J Eng Sci 10:623–641
16. Eringen AC (1990) Theory of thermo-microstretch elastic solids. Int J Eng Sci 28(12):1291–1301
17. Eringen AC (1992) Balance laws of micromorphic continua revisited. Int J Eng Sci 30(6):805–810
18. Eringen AC (1999) Microcontinuum field theories. Springer, Berlin Heidelberg New York
19. Eringen AC, Kafadar CB (1976) Polar field theories. In: Continuum physics, vol 4. Eringen AC (ed) Academic, New York, pp 1–73
20. Forest S, Sievert R (2003) Elastoviscoplastic constitutive frameworks for generalized continua. Acta Mech 160:71–111
21. Günther W (1958) Zur Statik und Kinematik des Cosserat'schen Kontinuums. Abh. Braunschweigische Wiss. Gesell. 10:195–213
22. Green AE, Rivlin RS (1964) Multipolar continuum mechanics. Arch Ration Mech Anal 17:113–147
23. Hill R (1998) The mathematical theory of plasticity. Clarendon, Oxford (reprint)
24. Iesan D, Nappa L (2001) On the plane strain of microstretch elastic solids. Int J Eng Sci 39:1815–1835
25. Iesan D, Nappa L (2001) Extremum principles and existence results in micromorphic elasticity. Int J Eng Sci 39:2051–2070
26. Iesan D, Quintanilla R (1994) Existence and continuous dependence results in the theory of microstretch elastic bodies. Int J Eng Sci 32:991–1001
27. Iesan D, Scalia A (2003) On complex potentials in the theory of microstretch elastic bodies. Int J Eng Sci 41(17):1989–2003
28. Kirchner, N, Steinmann, P (2005) A unifying treatise on variational principles for gradient and micro-morphic continua. Philosophical Magazine 85(33–35):3875–3895
29. Kumar R, Deswal, S (2002) Wave propagation through a cylindrical bore contained in a microstretch elastic medium. J Sound Vib 250(4):711–722
30. Lax PD, Milgram AN (1954) Parabolic equations. Contributions to the theory of partial differential equations. Ann Math Stud 33:167–190
31. Lee JD, Chen Y (2003) Constitutive relations of micromorphic thermoplasticity. Int J Eng Sci 41(17):387–399
32. Leslie FM (1968) Some constitutive equations for liquid crystals. Arch Ration Mech Anal 28:265–283
33. Marsden, JE, Hughes JR, Hughes TJR (1983) Mathematical Foundations of Elasticity. Prentice-Hall, Englewood Cliffs
34. Mindlin RD (1963) Microstructure in linear elasticity. Arch Ration Mech Anal 16:51–78
35. Mühlhaus HB (1989) Application of Cosserat theory in numerical solutions of limit load problems. Ing Arch 59:124–137
36. Mühlhaus HB, Vardoulakis I (1987) The thickness of shear bands in granular materials. Géotechnique 37:271–283
37. Nappa L (2001) Variational principles in micromorphic elasticity. Mech Res Commun 28:405–412
38. Neff P (2006) Existence of minimizers for a finite-strain micromorphic elastic solid. Proc R Soc Edinburgh, **A** 136:997–1012
39. Oden JT, Reddy JN (1976) Variational methods in theoretical mechanics. Springer, Berlin Heidelberg New York
40. Scalia A (2000) Extension, bending and torsion of anisotropic microstretch elastic cylinders. Math Mech Solids 5(1):31–40
41. Schwab C (1998) p- and hp- finite element methods. Theory and applications in solid and fluid mechanics. Clarendon Press, Oxford
42. Simo JC, Hughes TJR (1998) Computational inelasticity. Springer, Berlin Heidelberg New York
43. Singh B (2001) Reflection and refraction of plane waves at a liquid/thermo-microstretch elastic solid interface. Int J Eng Sci 39(5):583–598
44. Steeb H, Diebels S (2005) Continua with affine microstructure: theoretical aspects and applications. Proc Appl Math Mech 5:319–320
45. Steinmann P (1995) Theory and numerics of ductile micropolar elastoplastic damage. Int J Eng Sci 38:583–606
46. Steinmann P (1999) Formulation and computation of geometrically nonlinear gradient damage. Int J Numer Methods Eng 46:757–779
47. Toupin RA (1962) Elastic materials with couple stress. Arch Ration Mech Anal 11:385–413
48. Toupin RA (1964) Theory of elasticity with couple stresses. Arch Ration Mech Anal 17:85–112
49. Truesdell C, Noll W (1965) The non-linear field theories of mechanics. In: Flügge S (ed) Encyclopedia of Physics III/3. Springer, Berlin Heidelberg New York
50. Zienkiewicz OC, Taylor RL (1989,1991) The finite element method, 4th edn, vols 1 and 2. McGraw Hill, New York